CLASSIFYING COLOR TRANSITIONS INTO SHADOW-GEOMETRY, ILLUMINATION, HIGHLIGHT OR MATERIAL EDGES

T. Gevers and H.M.G. Stokman

Faculty of Science, University of Amsterdam
Kruislaan 403, 1098 SJ Amsterdam, The Netherlands
{gevers, stokman}@wins.uva.nl

ABSTRACT

We aim at using color information to classify the physical nature of a color edge: that is whether the transition is due to shadows, abrupt surface orientation changes, illumination, highlights or material changes. To achieve physics-based edge classification, we propose a taxonomy of color invariant edges. The taxonomy is based upon the sensitivity of the various color edges with respect to different imaging dependencies i.e. shadows, object shape, shading (i.e. illumination intensity changes), highlights and material characteristics. From this taxonomy, the edge classifier is derived labeling color transitions into the following types: (1) shadow, geometry or shading edges, (2) highlight edges, (3) material edges. Experiments conducted with the edge classification technique on color and hyperspectral images show that the proposed method successfully discriminates the different edge types.

1. INTRODUCTION

Discriminating edge types, based on their reflectance properties, is useful for a number of applications such as object recognition, stereo vision and structure from motion, where similar edge types (e.g. material transitions) from two distinct images are used for image matching while discounting other "accidental" edge types (e.g. shadows and highlight transitions).

Various physics-based segmentation schemes have been proposed [1], [3], [4], for example. Although these techniques rely on physics-based considerations to obtain segmentation results independent of the varying imaging conditions, they do not classify color transitions into different transition types.

Therefore, in this paper, we first propose computational models to compute color invariant edges. Then, a new color edge taxonomy is presented based upon the sensitivity of different color edges with respect to the following imaging dependencies: shadows, object shape, illumination, highlights, and material characteristics. From this taxonomy, the color edge classifier is derived. In this paper, we focus on color images recorded by a standard ccd camera and hyperspectral images recorded by a spectrograph, transforming the CCD camera into a line scanner: One axis contains the spatial information, whereas the other axis contains 60 spectral samples in the visible wavelength range.

The paper is organized as follows. In Section 2, different color models are presented. In Section 3, computational methods are proposed to compute color invariant gradients. Next, in Section 4, the classification scheme is presented to classify edges based on their reflectance characteristics. Experiments are conducted in Section 5. Finally, several conclusions will be drawn.

2. COLOR INVARIANT MODELS

In Gevers and Smeulders [2], color models have been proposed which have some degree of invariance for the purpose of object recognition. In this paper, we use the different color models for the purpose of color edge classification. We focus on $c_1c_2c_3$ defined by:

$$c_1 = \arctan(\frac{R}{\max\{G,B\}}) \tag{1}$$

$$c_2 = \arctan(\frac{G}{\max\{R,B\}}) \tag{2}$$

$$c_3 = \arctan(\frac{B}{\max\{R,G\}}) \tag{3}$$

and $l_1l_2l_3$ defined by:

$$l_1 = \frac{|R-G|}{|R-G|+|R-B|+|G-B|} \tag{4}$$

$$l_2 = \frac{|R-B|}{|R-G|+|R-B|+|G-B|} \tag{5}$$

$$l_3 = \frac{|G-B|}{|R-G|+|R-B|+|G-B|} \quad (6)$$

The effect of varying imaging circumstances have been analyzed for dichromatic reflectance differentiated for RGB, $c_1c_2c_3$ and $l_1l_2l_3$ [2]. From this analysis it has been shown that $l_1l_2l_3$ varies with a change in material only, $c_1c_2c_3$ with a change in material and highlights, and RGB varies with a change in material, highlights, shading and object shape.

3. COLOR INVARIANT GRADIENTS

In the previous section, color models have been discussed. In this section, we present color invariant edges derived from the various color models.

3.1. Gradients in multi-valued images

We follow the principled way to compute gradients in vector images as described by Silvano di Zenzo [5] and further used in [6], which is summarized as follows.

Let $\Theta(x_1,x_2) : \Re^2 \rightarrow \Re^m$ be a m-band image with components $\Theta_i(x_1,x_2) : \Re^2 \rightarrow \Re$ for $i = 1,2,...,m$. For color images recorded by the ccd color camera we have $m = 3$. For the hyperspectral images taken by the spectrograph we have $m = 60$. Hence, at a given image location the image value is a vector in $\Re^m$. The difference at two nearby points $P = (x_1^0, x_2^0)$ and $Q = (x_1^1, x_2^1)$ is given by $\triangle\Theta = \Theta(P) - \Theta(Q)$. Considering an infinitesmall displacement, the difference becomes the differential $d\Theta = \sum_{i=1}^{2} \frac{\partial\Theta}{\partial x_i} dx_i$ and its squared norm is given by:

$$d\Theta^2 = \sum_{i=1}^{2}\sum_{k=1}^{2} \frac{\partial\Theta}{\partial x_i}\frac{\partial\Theta}{\partial x_k} dx_i dx_k = \sum_{i=1}^{2}\sum_{k=1}^{2} g_{ik} dx_i dx_k =$$

$$\begin{bmatrix} dx_1 \\ dx_2 \end{bmatrix}^T \begin{bmatrix} g_{11} & g_{12} \\ g_{21} & g_{22} \end{bmatrix} \begin{bmatrix} dx_1 \\ dx_2 \end{bmatrix} \quad (7)$$

where $g_{ik} := \frac{\partial\Theta}{\partial x_i} \cdot \frac{\partial\Theta}{\partial x_k}$ and the extrema of the quadratic form are obtained in the direction of the eigenvectors of the matrix $[g_{ik}]$ and the values at these locations correspond with the eigenvalues given by:

$$\lambda_\pm = \frac{g_{11} + g_{22} \pm \sqrt{(g_{11}-g_{22})^2 + 4g_{12}^2}}{2} \quad (8)$$

with corresponding eigenvectors given by $(\cos\theta_\pm, \sin\theta_\pm)$, where $\theta_+ = \frac{1}{2}\arctan\frac{2g_{12}}{g_{11}-g_{22}}$ and $\theta_- = \theta_+ + \frac{\pi}{2}$. Hence, the direction of the minimal and maximal changes at a given image location is expressed by the eigenvectors θ_- and θ_+ respectively, and the corresponding magnitude is given by the eigenvalues λ_- and λ_+ respectively. Note that λ_- may be different than zero and that the strength of an multi-valued edge should be expressed by how λ_+ compares to λ_-, for example by subtraction $\lambda_+ - \lambda_-$ as proposed by [6], which will be used to define gradients in multi-valued color *invariant* images in the next section.

3.2. Gradients in multi-valued color invariant images

In this section, we propose color invariant gradients based on the multi-band approach as described in the previous section. For the ease of illustration, we focus on $m = 3$. Edge computation from hyperspectral (invariant) images, with $m = 60$, is straight forward.

The color gradient for RGB is as follows:

$$\nabla\mathcal{C}_{RGB} = \sqrt{\lambda_+^{RGB} - \lambda_-^{RGB}} \quad (9)$$

for

$$\lambda_\pm = \frac{g_{11}^{RGB} + g_{22}^{RGB} \pm \sqrt{(g_{11}^{RGB} - g_{22}^{RGB})^2 + 4(g_{12}^{RGB})^2}}{2} \quad (10)$$

where $g_{11}^{RGB} = |\frac{\partial R}{\partial x}|^2 + |\frac{\partial G}{\partial x}|^2 + |\frac{\partial B}{\partial x}|^2$, $g_{22}^{RGB} = |\frac{\partial R}{\partial y}|^2 + |\frac{\partial G}{\partial y}|^2 + |\frac{\partial B}{\partial y}|^2$, $g_{12}^{RGB} = \frac{\partial R}{\partial x}\frac{\partial R}{\partial y} + \frac{\partial G}{\partial x}\frac{\partial G}{\partial y} + \frac{\partial B}{\partial x}\frac{\partial B}{\partial y}$.

Further, we propose that the color invariant gradient (based on $c_1c_2c_3$) for matte objects is given by:

$$\nabla\mathcal{C}_{c_1c_2c_3} = \sqrt{\lambda_+^{c_1c_2c_3} - \lambda_-^{c_1c_2c_3}} \quad (11)$$

for

$$\lambda_\pm = \frac{g_{11}^{c_1c_2c_3} + g_{22}^{c_1c_2c_3} \pm \sqrt{(g_{11}^{c_1c_2c_3} - g_{22}^{c_1c_2c_3})^2 + 4(g_{12}^{c_1c_2c_3})^2}}{2} \quad (12)$$

where $g_{11}^{c_1c_2c_3} = |\frac{\partial c_1}{\partial x}|^2 + |\frac{\partial c_2}{\partial x}|^2 + |\frac{\partial c_3}{\partial x}|^2$, $g_{22}^{c_1c_2c_3} = |\frac{\partial c_1}{\partial y}|^2 + |\frac{\partial c_2}{\partial y}|^2 + |\frac{\partial c_3}{\partial y}|^2$, $g_{12}^{c_1c_2c_3} = \frac{\partial c_1}{\partial x}\frac{\partial c_1}{\partial y} + \frac{\partial c_2}{\partial x}\frac{\partial c_2}{\partial y} + \frac{\partial c_3}{\partial x}\frac{\partial c_3}{\partial y}$.

Similarly, we propose that the color invariant gradient (based on $l_1l_2l_3$) for shiny objects is given by:

$$\nabla\mathcal{C}_{l_1l_2l_3} = \sqrt{\lambda_+^{l_1l_2l_3} - \lambda_-^{l_1l_2l_3}} \quad (13)$$

for

$$\lambda_\pm = \frac{g_{11}^{l_1l_2l_3} + g_{22}^{l_1l_2l_3} \pm \sqrt{(g_{11}^{l_1l_2l_3} - g_{22}^{l_1l_2l_3})^2 + 4(g_{12}^{l_1l_2l_3})^2}}{2} \quad (14)$$

where $g_{11}^{l_1l_2l_3} = |\frac{\partial l_1}{\partial x}|^2 + |\frac{\partial l_2}{\partial x}|^2 + |\frac{\partial l_3}{\partial x}|^2$, $g_{22}^{l_1l_2l_3} = |\frac{\partial l_1}{\partial y}|^2 + |\frac{\partial l_2}{\partial y}|^2 + |\frac{\partial l_3}{\partial y}|^2$, $g_{12}^{l_1l_2l_3} = \frac{\partial l_1}{\partial x}\frac{\partial l_1}{\partial y} + \frac{\partial l_2}{\partial x}\frac{\partial l_2}{\partial y} + \frac{\partial l_3}{\partial x}\frac{\partial l_3}{\partial y}$.

In the next section, the color invariant gradients will be used to discriminate the different edge types by their physical nature.

4. PHYSICS BASED EDGE CLASSIFICATION

From the previous sections and [2], we may conclude that $\nabla\mathcal{C}_{RGB}$ measures the presence of (1) shadow, shading or geometry edges, (2) highlight edges, (3) material edges. Further, $\nabla\mathcal{C}_{c_1c_2c_3}$ measures the presence of (2) highlight edges, (3) material edges. And $\nabla\mathcal{C}_{l_1l_2l_3}$ measures the presence of only (3) material edges. As a result, a taxonomy of color edges can be given, see Fig. 1.

	shape edges	shadow edges	highlight edges	material edges
∇C_{RGB}	+	+	+	+
∇C_{c1c2c3}	-	-	+	+
∇C_{l1l2l3}	-	-	-	+

Fig. 1. *Taxonomy of color edges based upon the sensitivity of the different color edges with respect to the different imaging conditions. - denotes invariant and + denotes sensitivity of the color edge to the imaging condition.*

Based on the given color edge taxonomy, we now present a color edge classifier discriminating edges in one of the following types: (1) shadow, shading or geometry edges, (2) highlight edges, (3) material edges.

Let the set of image coordinates of local RGB edge maxima in an image be denoted by E, which will be zero except at RGB edges. Then the rule-based reflectance classifier is as follows:

IF $(\nabla\mathcal{C}_{RGB}) > t_1$ AND $(\nabla\mathcal{C}_{c_1c_2c_3}) \leq t_2$
THEN classify as **shadow or geometry edge**
ELSE
IF $(\nabla\mathcal{C}_{c_1c_2c_3}) > t_2$ AND $(\nabla\mathcal{C}_{l_1l_2l_3}) \leq t_3$
THEN classify as **highlight edge**
ELSE
IF $(\nabla\mathcal{C}_{l_1l_2l_3}) > t_3$
THEN classify as **material edge**

only computed at RGB edge maxima where $\nabla\mathcal{C}_{RGB}$ is cf. eq. (9), $\nabla\mathcal{C}_{c_1c_2c_3}$ is cf. eq. (11), $\nabla\mathcal{C}_{l_1l_2l_3}$ is cf. eq. (13). Further, t_i are thresholds based on the noise level to suppress marginally visible edges. Automatic threshold setting is proposed in Stokman and Gevers [7].

5. EXPERIMENTS

5.1. The first recording: RGB image

Figure 3.a contains an image of several toys against a background consisting of four squares with distinct color. The size of the image is 256x256. The first upper left quadrant consists of three homogeneously painted matte cubes of wood. The second upper right quadrant contains two specular plastic donuts on top of each other. In the bottom left quadrant a red highlighted ball and a matte cube are shown while the last quadrant contains two matte cubes. The image is clearly contaminated by shadows, shading, highlights and shading. Note that each individual object is painted homogeneously with a distinct color.

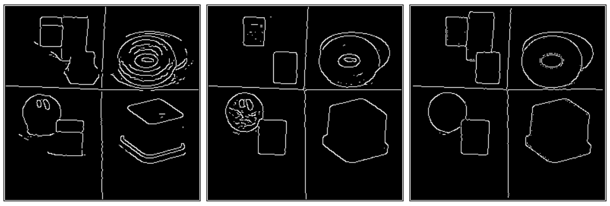

Fig. 2. *Edge maps of the various color models computed from the recorded color image shown in Figure 3.a. a. Edge map based on RGB gradient field $\nabla\mathcal{C}_{RGB}$ with non-maximum suppression. b. Edge map based on $c_1c_2c_3$ gradient field $\nabla\mathcal{C}_{c_1c_2c_3}$ with non-maximum suppression. c. Edge map based on $l_1l_2l_3$ gradient field $\nabla\mathcal{C}_{l_1l_2l_3}$ with non-maximum suppression.*

In Figure 2.a, edges are shown obtained from the RGB image. Clearly, edges are introduced by abrupt surface orientations, shadows, shading and highlights. In contrast, computed edges for $c_1c_2c_3$ and $l_1l_2l_3$ defined by $\nabla\mathcal{C}_{c_1c_2c_3}$ and $\nabla\mathcal{C}_{l_1l_2l_3}$ respectively, shown in Figure 2.b and 2.c, are insensitive for shadows, shading and surface orientation changes. In Figure 2.c, the edge map is shown for $l_1l_2l_3$ with non-maximum suppression. Good performance is shown where the computed edges correspond to material boundaries discounting the disturbing influences of surface orientation, illumination, shadows and highlights. Only inter-reflections disturb the quality of the edge map slightly (note that $l_1l_2l_3$ is not robust to inter-reflections).

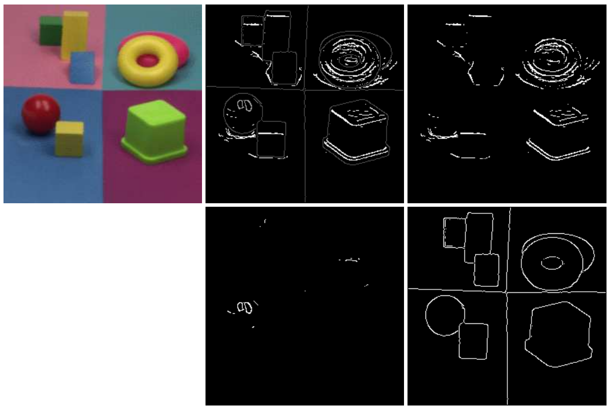

Fig. 3. *a. First recorded color image. b. Reflectance based edge classification. c. shadow and geometry edges d. highlight edges e. material transitions.*

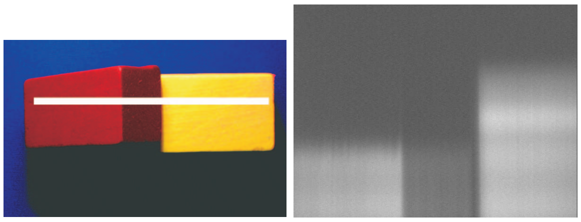

(a) (b)

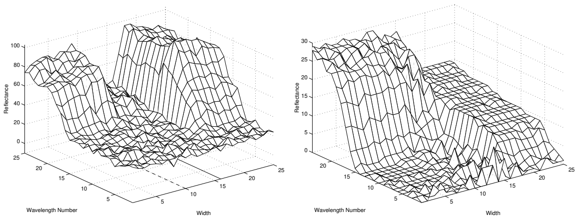

(a) (b)

Fig. 4. *a: Red and yellow wooden block. One side of the red block is shaded A region is marked in white from which a hyper-spectral line-scan image is taken, which is shown in b. Here, the top of the vertical axis corresponds to 400 nm, the bottom line corresponds to 700 nm. The horizontal axis represent spatial information.*

Fig. 5. *a: 3-D graph of the downsampled linescan image of Fig. 4b. The x-axis of the graph represents spatial data, the y-axis the spectral data, and the z-axis the reflectance of the objects. b: The normalized spectra of Fig. a is identical for the entire range of the red object. The detected and classified shadow or geometry edges are denoted by the dashed line at the bottom of the graph, the detected and classified material edge is shown as a solid line in Fig. 5.a.*

The edge classification results are shown in Figure 3.b for the color image shown in Figure 3.a. The edge classifier discriminates edges in the color image to be one of the following types: (1) shadow or geometry edges shown in Figure 3.c, (2) highlight edges shown in Figure 3.d, (3) material edges shown in Figure 3.e. From the observed results, the edge classifier discriminates the three edge types successfully. Only minor performance is achieved when intensity and highlights change smoothly over a wide image range due to the local behavior of the edge classifier.

5.2. The second recording: spectral image

In Fig. 4a, a red and a yellow wooden block are shown. The red block is oriented such that one side is shaded. A region is marked in white from which a hyper-spectral line-scan image is taken. Hyperspectral images are obtained using the Imspector V7 spectrograph, Jain CV-M300 camera and Matrox Corona Framegrabber, under Philips Practitone A60 Daylight illumination. The hyper-spectral image is shown in Fig. 4b. The hyper-spectral image of 760 x 580 pixels is filtered along the spectral axis with a uniform filter of size 9, after which 25 samples are taken in the 450 - 700 nm range. This spectral line scan image thus has a dimension of 760 x 1 x 25. A visually comprehensive representation of the sampled linescan image of Fig. 4b is shown in Fig. 5a where both the spectral and spatial information are downsampled.

Based on comparison of the edge maps from raw hyperspectra and from normalized hyper-spectra, shadow-geometry edges and material edges can be distinguished. This is demonstrated in Fig. 5.b where the normalized spectra are identical for the entire range of the red object. As a result, an edge detector finds the material edge. In contrast, the edge detector operating on the spectrum of Fig. 5a finds the shadow and material edge. The combination of the edge maps thus distinguishes a shadow/geometry (dashed line at bottom of Fig. 5a) from a material edge (solid line) from spectral information.

6. CONCLUSION

In this paper, color information is used to classify the physical nature of the color transitions. To this end, a taxonomy of color invariant edges has been proposed. From the taxonomy the edge classifier has been derived. Experiments conducted with the edge classification technique on color and hyperspectral images show that the proposed method successfully discriminates the different edge types.

7. REFERENCES

[1] Bajcsy, R., Lee S. W., and Leonardis, A., *Color Image Segmentation with Detection of Highlights and Local Illumination Induced by Inter-reflections*, ICPR, pp. 785-790, NJ, 1990.

[2] Gevers, T and Smeulders, A.W.M., *Color Based Object Recognition*, Pattern Recognition, 32, pp. 453-464, 1999.

[3] Healey, G., *Segmenting Images Using Normalized Color*, IEEE Syst., Man. Cybern., Vol. 22, pp. 64-73, 1992.

[4] Klinker, G. J., Shafer, A. and Kanada, T., *A Physical Approach to Color Image Understanding*, Int. J. of Comp. Vision, Vol. 4, pp. 7-38, 1990.

[5] di Zenzo, S., *Gradient of a Multi-images,* CVGIP, 33:116-125, 1986.

[6] Sapiro, G, Ringach, D.L., *Anisotropic Diffusion of Multi-valued Images with Applications,* to Color Filtering, IEEE PAMI, (5)11, 1582-1586, 1996.

[7] Stokman, H. and Gevers, T., *Hyperspectral Edge Detection and Classification*, BMVC, Nottingham, September, 1999